Structural evolution of the Arunachal Himalaya and implications for asymmetric development of the Himalayan orogen

A. Yin[1,*], C. S. Dubey[2], T. K. Kelty[3], G. E. Gehrels[4], C. Y. Chou[1], M. Grove[1] and O. Lovera[1]

[1]Department of Earth and Space Sciences and Institute of Geophysics and Planetary Physics, University of California, Los Angeles, CA 90095-1567, USA
[2]Department of Geology, University of Delhi, Delhi 110 007, India
[3]Department of Geological Sciences, California State University, Long Beach, California 90840-3902, USA
[4]Department of Geosciences, University of Arizona, Tucson, Arizona 85721, USA

Geologic mapping and stratigraphic correlation of low-grade Precambrian Lesser Himalayan units using U–Pb detrital zircon dating reveal the existence of a Main Central Thrust (MCT) window and a prominent ductile thrust zone within the Greater Himalayan Crystallines in the Arunachal Himalaya of NE India. The newly discovered MCT window is cut and offset by several active north-trending normal faults extending from southeast Tibet, indicating the fault is no longer active. Ion-microprobe dating of monazite inclusions in garnets from the MCT zone indicates that the fault was active at 10.1 ± 1.4 Ma. Our structural data together with a synthesis of existing geologic maps suggest that the eastern Himalaya is composed of a large thrust duplex with the folded MCT as the roof fault. The total amount of crustal shortening accommodated by the duplex and the MCT south of the South Tibetan Detachment may exceed 500 km, which is probably greater than the amount of crustal shortening across the central Himalaya in Nepal and definitely greater than the amount of shortening across the western Himalaya in Pakistan. The observed systematic variation of crustal shortening suggests that Himalayan crustal thickening and uplift are uneven along strike, which may be in response to the westward decrease in convergence rate between India and Asia during the Cenozoic.

Keywords: Arunachal Himalaya, Himalayan orogen, Main Central Thrust, zircon dating.

THE Himalayan orogen was created by the Cenozoic Indo-Asian collision[1]. The geology of its western and central segments west of Bhutan is quite well known, due to extensive geologic investigations over the past several decades[1–7]. In the central Himalaya, the major faults (i.e. the Main Frontal Thrust, MFT; Main Boundary Thrust, MBT; Main Central Thrust, MCT, South Tibet Detachment, STD) juxtapose laterally continuous tectonostratigraphic units for over 1000 km (i.e. Greater Himalayan Crystalline Complex, GHC; Lesser Himalayan Sequence, LHS; Tethyan Himalayan Sequence, THS and the sub-Himalayan belt)[8]. In contrast, significant along-strike variation in lithology and metamorphic grades occurs in northern Pakistan and northwestern India of the western Himalaya, where the magnitude of crustal shortening is significantly less than that in the central Himalaya, as indicated by correlative lithologic units across major faults and change in metamorphic grades in both the hanging wall and footwall of the MCT along strike[9–12]. An obvious question from these first-order observations is whether the Himalayan orogen was constructed in the same manner along its whole length with a constant magnitude of crustal shortening or varies along strike of the orogen in response to a westward decrease in convergence rate between India and Asia[13,14]. In addition, it is important to know if the Himalayan orogen was constructed synchronously or diachronously along strike. We address these questions below by presenting newly obtained geologic and geochronological data from the Arunachal Himalaya of NE India.

Geology of the Arunachal Himalaya

The Arunachal Himalaya occupies the easternmost segment of the Himalaya between long. 91°30′E and 96°E, and includes the eastern Himalayan syntaxis (Figure 1). This segment of the Himalaya is located east of Bhutan, where Gansser[15] and Indian Geological Survey[16] have done extensive mapping. Geologic research in the Arunachal Himalaya can be traced back to the 19th century during which several reconnaissance investigations were conducted along its foothills[17–20]. The early research laid a foundation for a proliferation of geologic activities[20–24] in the early 1970s and subsequent regional syntheses by Thakur[25], Singh and Chowdhary[26], Acharyya[27–29], and Kumar[30], among others. These overviews establish general stratigraphy

*For correspondence. (e-mail: yin@ess.ucla.edu)

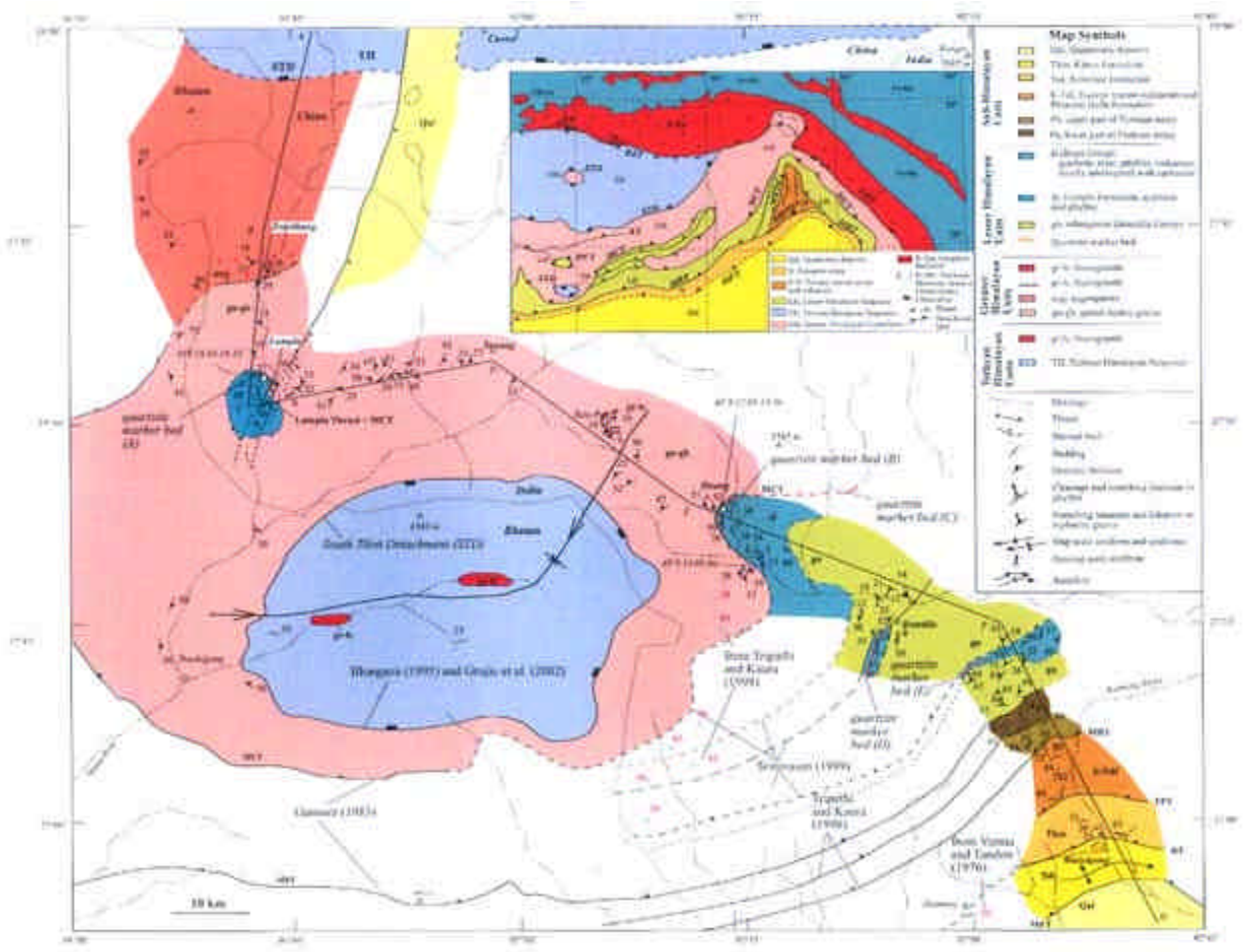

Figure 1. Tectonic sketch of the eastern Himalaya. Imbricate thrusts in Lesser Himalaya based on this study, STD klippe from Grujic *et al.*[4], eastern-syntaxis geology from Ding *et al.*[58] and Geological Survey of India[32], MCT and MBT traces from Singh and Chawdhary[26], Tripathi and Kaura[59] and this study. The geology of southeast Tibet is from Yin and Harrison[60]. Attitude from Verma and Tandon[22], and Tripathi and Kaura[59] are shown with red and brown numbers on the map. *Inset*, Geologic map of eastern Bhutan and western Arunachal Himalaya and location of cross-section shown in Figure 3. Traces of the STD and MCT and strikes and dips of bedding and foliation in eastern Bhutan are from refs 4, 15, 16. MFT, Main Frontal Thrust; BT, Bhalukpung Thrust; TFT, Tipi Thrust; MBT, Main Boundary Thrust; MCT, Main Central Thrust; ZT, Zimithang Thrust.

and tectonic framework of the region and place the major lithologic units in the context of the overall Himalayan tectonic framework[21,22,26,27,30,31]. Noticeably, past investigations in the region are almost entirely based on field studies without application of modern geochronology and quantitative structural analyses. As a result, the age of the major lithologic units are highly uncertain and we know almost nothing about the timing of exhumation of the region and the age of fault motion along major structures such as the MCT. For example, few igneous units in the Arunachal Himalaya have been dated radiometrically[30]. In addition, our understanding of the basic structural geology of the region remains incomplete. For example, even the basic geometry of the MCT has been portrayed differently either as a simple north-dipping fault or a folded thrust[26,30,32]. Below we describe our observations along a traverse across the westernmost Arunachal Himalaya and present new geochronologic data that provide general constraints on the age and correlation of the Lesser Himalayan sequence in the region and timing of motion on the MCT.

Structure and stratigraphy

The MFT as the contact between the Brahmaputra alluvium and the sub-Himalaya is concealed by vegetation and Holocene deposits along our traverse. Cenozoic strata in the hanging wall are broadly folded (Figures 1 and 2) and were assigned as the Plio-Pleistocene Kimin and Subansiri Formations[26,30]. The north-dipping Bhalukpong thrust observed in this study and the Tipi thrust[26,27] lie within the Tertiary strata. The Tipi thrust juxtaposes the Dafla Formation over the Kimin and Subansiri Formations. It strikes N45°E and dips 55°NW with down-dip striations. Acharyya[27,29] reported that Eocene marine strata and volcanics are distributed along the MBT and Tipi zones, tectonically juxtaposed either on the top or bottom of the Dafla Formation sandwiched between the two thrusts. He envisioned that the Eocene strata formed as thrust horses in a duplex system below the MBT. In Figures 1 and 2, we lump the Eocene and Dafla strata as a single unit.

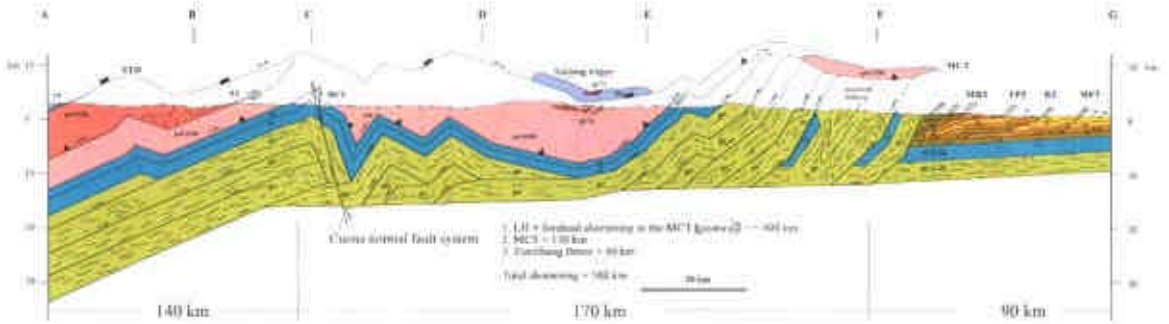

Figure 2. Geologic cross-section of western Arunachal Himalaya.

The MBT is not exposed, but its location is well determined. Its hanging-wall Permian and footwall Tertiary strata are isoclinally folded and sheared by mesoscopic thrusts. Locally bedding in Permian strata is completely transposed by axial cleavage. Acharyya *et al.*[23] divided the Permian strata into three units separated by thrusts. The threefold division was later simplified into two divisions by the Geological Survey of India[32] that is followed in our cross-section construction. Placing a thrust between the structurally upper and lower Permian units is consistent with our observations that the units have different attitudes across the inferred thrust (Figure 2).

The north-dipping Permian strata lie below augen gneiss interlayered with phyllite, quartzite, metavolcanics and carbonates, collectively known as the Bomdila Group (Figure 2)[30]. Mylonitic fabrics are widely developed in the gneiss, as reported by Verma and Tandon[22]. We are not aware of any other kinematic analysis of the mylonitic rocks. Our field observations consistently suggest that the north-trending stretching lineation has top-south sense of shear as indicated by S–C fabrics and asymmetric porphyroblasts. This kinematics is consistent with regional top-south Cenozoic thrusting such as along the MCT and MBT. This kinematic compatibility strongly suggests that the mylonitic shear zones within the Bomdila gneiss are Cenozoic in age, developed during the formation of the Lesser Himalayan thrust belt.

Structurally above the Bomdila Group is a sequence of phyllite and quartz arenite, locally interbedded with carbonate. They are commonly referred to as the Tenga Formation and Rupa Group[30,33,34]. A distinctive marker bed is present in this unit, namely the Miri Quartzite, which can be traced across the whole Arunachal Himalaya[21,34,35]. This marker bed is duplicated several times based on our own observations and those by Verma and Tandon[22] (Figure 1). The youngest age of the detrital zircons in the Rupa Group is about 950 Ma (see more detailed description below), suggesting that its deposition must have occurred after this time. The age of the Bomdila gneiss was dated by the whole-rock Rb/Sr isochron method from samples collected near Bomdila, which yielded 1644 ± 40 Ma and 1676 ± 122 Ma, respectively[36]. Later geochronological analysis of the Bomdila augen gneiss by Dikshitulu *et al.*[37] using the Rb/Sr method with a six-point isochron indicates its age to be 1914 ± 23 Ma. These authors also report a 1536 ± 60 Ma Rb/Sr age for a high-Ca granite that intrudes into the dark grey phyllite. From the above age constraints, we may conclude that there are at least four chronologic units in the Arunachal Lesser Himalayan Sequence; two are igneous and two metasedimentary. The oldest rock could either be the 1914 Ma gneiss or the metasedimentary sequence that is intruded by the ~1530 Ma granite. The ~1530 Ma granite may be produced by a protracted igneous event lasting from ~ 1676 to 1530 Ma and be part of the main body of the Bomdila gneiss complex. The youngest nonfossiliferous Lesser Himalayan unit is the Rupa Group, which must be younger than 950 Ma as constrained by our detrital zircon ages. Because of a large age gap between the Bomdila gneiss and the Rupa Group, we suggest that the latter was deposited unconformably on top of the Bomdila gneiss. As shown below, the detrital zircon ages from the Rupa Group are clustered at ~1400 and 1700 Ma, respectively. These ages are broadly compatible with those from the Bomdila gneiss and may further suggest that the Bomdila gneiss is the basement and source of the detrital zircons for the Rupa Group.

The MCT near Dirang juxtaposes garnet-bearing gneiss and kyanite-bearing schist over phyllite, quartzite and metavolcanic rocks. The fault zone is ~100–300 m thick and consists of mesoscopic folds trending N5°W to N45°W and verging to both southwest and northeast. As the folds are subparallel to striations dominantly trending N10–20°W in the MCT zone, the fold hinges may have been rotated into sub-parallelism to the thrust transport direction during shear along the MCT. Although we observed no mylonitic shear zones associated with the MCT, a weak stretching lineation trending about N5–15°W is locally present in phyllite below the thrust. From the MCT zone upward, the number and size of deformed and undeformed leucogranites increase. At the base of the MCT hanging wall, the leucogranites are less than tens of centimetre thick and a few metres long. However, at higher levels near Se La pass (Figure 1), they increase to 20–40 m thick and >100 m long. Associated with the large quantity

of leucogranites near Se La pass is the appearance of sillimanite, indicating upward increase in metamorphic grade.

We mapped a warped, low-angle fault near Lumla between Tawang and Zhimithang, which we term as the Lumla thrust. This fault places high-grade garnet–biotite gneiss over low-grade phyllite and quartz arenite (Figure 1). The latter is similar to phyllite and quartz arenite of the Rupa unit we observed to the south in the footwall of the MCT. The fault has a 1–3 m thick gouge zone, with stretching lineation trending N30–50°W in footwall phyllite. Southeast-verging folds are present below the fault with hinges trending between N30°E/S30°W and N75°E/S75°W. These observations indicate a top-southeast sense shear on the Lumla thrust. According to Kumar[30] and the Arunachal geologic map, phyllite and arenite near Lumla belong to the basal part of the Tethyan Himalayan Sequence (THS) that rests unconformably on top of the Greater Himalayan Crystalline Complex (GHC). This interpretation is inconsistent with our field observations that the high-grade rocks are juxtaposed against low-grade rocks. The Lumla thrust is offset between 5 and 200 m by several north-striking normal faults (Figure 1).

The LHS strata in Lumla could either be an embayment of a half window or a full window of the MCT. Due to the difficult access around Lumla, we were not able to trace the fault and the interpreted Rupa strata laterally. However, our preliminary interpretation of the available LANDSAT image and extrapolation of the known trace of the MCT in Bhutan led us to interpret that the occurrence of the LHS in Lumla results from the presence of an MCT window, which we refer to as the Lumla window. This hypothesis needs to be tested by future field mapping.

Our mapping also reveals a north-dipping mylonitic thrust shear zone (>150 m thick) near Zimithang in the GHC, that we term here as the Zimithang thrust (Figure 1). The shear zone places augen gneiss over garnet–biotite quartzo-feldspathic gneiss. Stretching lineation in the zone trends between N10°E and N45°W. The presence of this shear zone indicates significant internal shortening within the GHC by thrusting. From the location of the Zimithang shear zone, we correlate it to the north-dipping Kakhtang thrust in eastern Bhutan[4,15], which is also a prominent ductile thrust in the GHC.

U–Pb detrital zircon dating

The hanging-wall and footwall units across the Lumla thrust are remarkably similar to those across the frontal trace of the MCT near Dirang, raising the possibility that the Lumla thrust is a tectonic window of the MCT. To test this hypothesis and to determine whether the Lumla phyllite and arsenite belong to the THS, we conducted U–Pb dating of detrital zircons from two arsenite samples collected at Lumla and Dirang (AY 9.16.03.14-53 and AY 9.17.03.15-56 in Figure 1). The analyses were preformed by laser-ablation-ICPMS at University of Arizona. We dated 97 and 100 zircon grains respectively, for the two samples, both yielding similar $^{207}Pb/^{206}Pb$ age distributions ranging from ~950 to ~2960 Ma (Figure 3 *a* and *b*; Table 1). For both samples there are two prominent age clusters at 1400 and 1700 Ma, which are different from typical detrital zircon ages of the THS but similar to those from the LH determined in Nepal[38,39] (Figure 3 *c*). We also compare the two age distributions by plotting cumulative counts against the $^{207}Pb/^{206}Pb$ age (Figure 3 *d*), which again shows remarkable similarities between the two samples. To make the comparison statistically rigorous, we performed Kolmogorov–Smirnov analysis[40]. The results indicate that the distributions are distinguishable only at 60% confidence interval (30% confidence level for error-weighted analyses). Hence the null hypothesis cannot be disproved at a statistically significant level (i.e. 95% confidence level) and the two samples may very well come from the same source region.

Timing of motion on the Main Central Thrust

In order to determine the age of the MCT, we performed U–Th ion-microprobe dating of monazite inclusions in garnet from the MCT zone. The general analytical procedures are as follows. Monazite grains in polished thin sections from rock samples were located using backscattered electron (BSE) petrography (Figure 4) and energy-dispersive X-ray spectroscopy with a scanning electron microscope or an electron microprobe at UCLA. Monazites found in the matrices of rocks were not used to obtain ages. Only monazites in garnets were used in the *in situ* Th–Pb dating method. Monazite crystals were found to vary in size from 5 to 20 μm. Monazite grains in garnet were documented with detailed BSE images. The portion of the thin section that contained monazite grains and surrounding garnet was precisely cut using a precision table saw and mounted in epoxy with a minimum of ten grains of polished monazite age standards (monazite 554, see Harrison *et al.*[41]). A digital camera attached to an optical microscope was used to take reflected light images of the garnets that contain monazite grains so as to aid relocating the grains during ion microprobe sessions. Before probe sessions, the mounted epoxy samples were cleaned in soapy water, then distilled water and high-purity ultrasound cleanser. Later the samples were gold-coated.

Monazite grains were analysed using a CAMECA ims 1270 ion microprobe. The dating method takes advantage of the kinetic energy distribution of the Th and Pb ions sputtered from monazite using a primary oxygen (O^-) beam focused to a spot size that varied from ~5 to 30 μm in diameter. Greater the diameter, greater are the chances of detecting the *in situ* monazite grains during initial relocating of the grains on the samples. However, due to the

small sizes of the grains from Arunachal Pradesh, in our sessions we chose the beam diameter to be at 15 μm (see Harrison *et al.*[41,42] for details). The primary beam varied from 5 to 15 nA. A 50 eV energy window and an ~10 eV offset for Th^+ was used. The mass resolving power of the ion microprobe set at ~6000 allows all Th and Pb isotopes to be resolved from any other molecular interference. The O-beam sputtered less than a micron of the grain surface and the monazite grain of interest was located by the beam quickly. Each grain analysis was scheduled for ten runs and the whole procedure was completed in minutes. The uncertainty in the Th–Pb monazite ages reported here is limited by the reproduction of a calibration curve and is ± 1–2%.

The sample we analysed (AY91403-(8a)) was collected directly above the MCT near Dirang (Figure 1). U–Th ion-microprobe analysis of monazite inclusions yields an age of 10 ± 1.4 Ma (1 *s*) from five monazite grains included in four different syn-kinematic garnets (Figure 3). This age is slightly older than the U–Th monazite inclusion ages of ~7–3 Ma in central Nepal[43,44]. Since the monazites in this study are included in garnets and unlikely to experience high temperature (>650°C) conditions for an extended period, the interpretation that they experienced large amounts of ^{208}Pb diffusional loss is improbable. Therefore, an age of ~10 Ma from these monazites in the MCT hanging wall records crystallization ages and suggests that the MCT was active in the late Miocene.

Magnitude of crustal shortening

The magnitude of crustal shortening across the whole or parts of the Himalayan orogen has been estimated in northern Pakistan[10,45], NW India[46–48], south-central Tibet[49,50], and

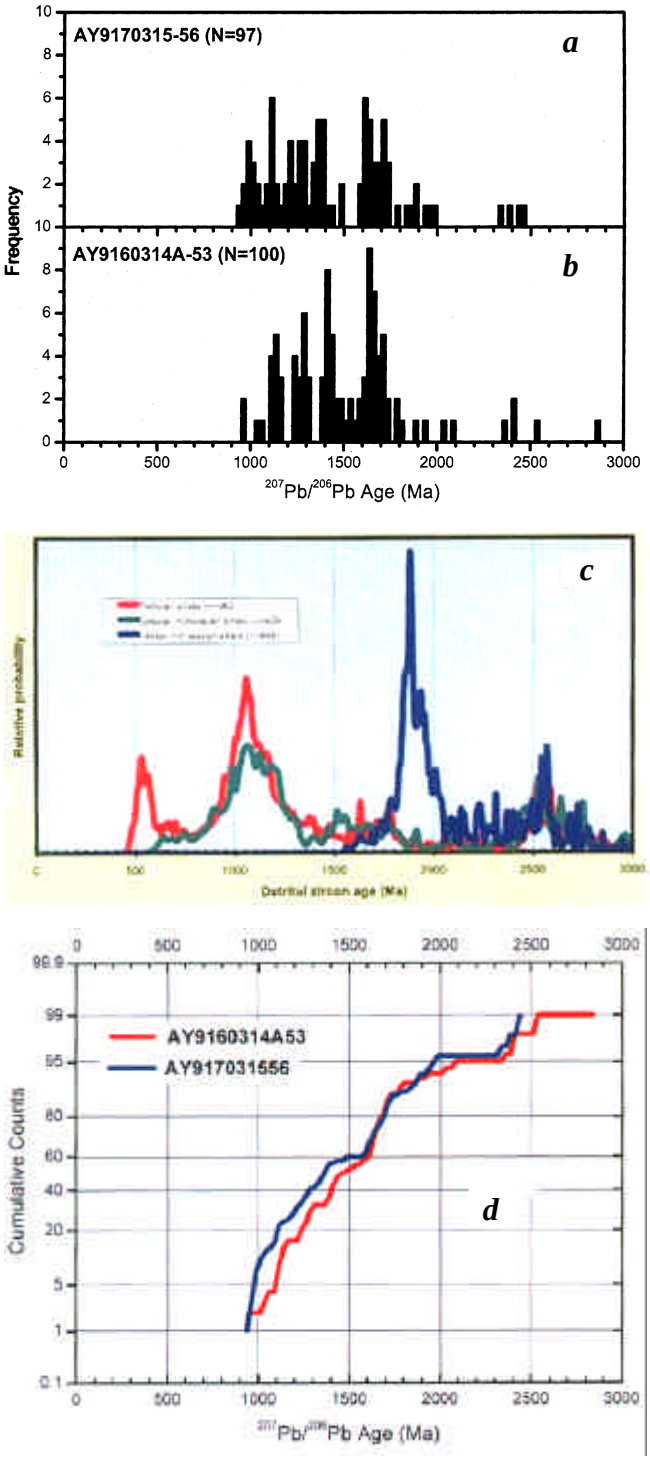

Figure 3. ***a***, Frequency diagram of $^{207}Pb/^{206}Pb$ detrital zircon ages for sample AY9170315-56. See Figure 1 *b* for sample location. ***b***, Frequency diagram of $^{207}Pb/^{206}Pb$ detrital zircon ages for sample AY9170314A-53. See Figure 1 *b* for sample location. ***c***, Comparison curves of detrital zircon ages from the Lesser Himalaya, Greater Himalaya, and Tethyan strata in Nepal[61]. ***d***, Cumulative probability plots of age distribution for samples AY9170315-56 and AY9170314A-53.

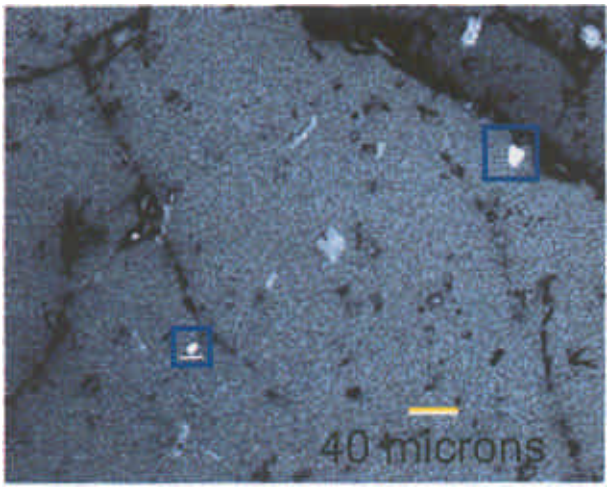

Figure 4. Back-scattered electron image of dated monazite inclusions in garnet from sample AY91403-(8a) from the MCT zone. See Figure 1 *b* for location.

Nepal[3,51] using balanced cross-sections. However, few such attempts have been made in the Arunachal Himalaya. Those who made balanced sections, focused their analysis exclusively on structures in the sub-Himalayan belt between the MBT in the north and the MFT zone in the south[27,29]. The existing balanced cross-section of Acharyya[27] in the Arunachal Himalaya implies ~30 km of shortening in the MBT footwall.

Following the early approaches in other parts of the Himalaya[3,47,48,50], we constructed a balanced cross-section across the westernmost Arunachal Himalaya by assuming kink-bend folding and constant bed thickness (Figure 2). Although this method produces folds with sharp hinges, it can also generate folds with circular hinge zones if the dip domains are close to one another as done in many cases of constructed balanced cross-sections[52]. One could easily smoothen the faults and contacts we draw in the cross section and make the fold hinges more rounded. We decided not to do this to allow the readers to directly evaluate our construction without introducing any arbitrary constructions. Also, as more field measurements are available, more realistic and detailed cross-sections can be constructed.

The most fundamental constraints on our cross-section are (1) surface geology (e.g. attitudes of beds, location of faults, etc.) we surveyed from Bhalukpong to Zhimithang (Figure 1), (2) thickness of the stratigraphic units determined from field mapping and (3) a regional dip of 3.5° of Indian basement beneath the Arunachal Himalaya as constrained by regional gravity data and modelling[53]. In our cross-section, the MBT has a relatively steep angle, which is inferred from the steeply dipping bedding attitudes immediately above the fault. Acharyya[27] has long advocated that the MBT is a flat-lying but folded thrust with a large magnitude of displacement. This is certainly a possibility, but implementing this type of geometry in our cross-section would violate measured bedding attitudes, assuming no out-of-sequence thrusting has occurred across the MBT zone. Without further constraints on deep crustal geometry of the MBT, we adopt a relatively simple geometry of the MBT as portrayed in our section that is permissible by all available geological data (Figure 2).

In our cross-section we project the STD and MCT mapped to the west and east of our field area onto our cross-section[4,26] (Figures 1 and 4). We also corrected the apparent line length with respect to the thrust transport direction of S30°E and obtained a total amount of shortening exceeding 585 km across our traverse using the line-balance method[54]. This shortening is distributed by >195 km motion on the MCT, ~310 km thrusting and folding in the LH, ~90 km thrusting in the Permian and Cenozoic strata, and >50 km motion on the Zimithang Thrust. Note that although the Bomdila gneiss is shown as a one continuous unit in our cross-section, it should be regarded as a composite unit that includes the Bomdila gneiss and its interlayered metasedimentary units as seen in Bhutan for the equivalent rocks[15].

The main uncertainty of our line-balance calculations comes from that of the Lesser Himalaya. First, the available structural data in this domain remain sparse. Second, the assumption that thrust-related folding in this unit is accommodated by flexural slip in the Lesser Himalaya is questionable because the Bomdila gneiss and its interlayered metasedimentary strata are folded at least at outcrop scale by ductile shearing and isoclinal folding. Third, it remains unclear whether repetition of marker beds in the Lesser Himalaya[22,52] was caused by folding or imbricate thrusting. To resolve these problems, we adopted an alternative area-balance method[55], in which we use our own field observations to constrain the thickness of the Bomdila (~3.5 km) and Rupa (~3.2 km) Groups. We again assume that the basal decollement beneath the western Arunachal Himalaya dips 3.5° to the north, as inferred from regional gravity data[53]. Finally we assume that the MCT exhibits the geometry as portrayed in Figure 4. Using this method, we obtained a total amount of 279 km shortening in the Lesser Himalayan belt, which is about 30 km less than that of 310 km estimated by line balancing. This minor difference can be attributed to the lack of a steep ramp in the northernmost part of the section in our area-balancing calculation. Our estimated total shortening using area balancing in the LH is likely to be a minimum because the estimated thicknesses of the Bomdila and Rupa Groups represent their upper bounds due to distributed thickening by internal folding and thrusting.

Discussion

The minimum crustal shortening estimated in the central Himalaya ranges from 185 to 245 km in eastern Nepal[51] and 418 to 493 km in western Nepal[3]. These do not include shortening in the Tethyan Himalaya above the STD. Farther west in northern Pakistan, DiPietro and Pogue[10] estimated shortening across the westernmost Himalaya to be ~200 km and suggested a westward decrease in contraction from the central Himalaya compared to the estimates in Nepal[3,50,51]. Although our estimated minimum crustal shortening is significantly greater than that estimated from the western Himalaya, comparing our estimates against those from the Nepal Himalaya requires qualification, because both estimates are minimum values. The main cause of the lower-bound estimates in Nepal and our study area is due to erosion of hanging-wall cut-offs. If this is the case, then we may partition the total amount of shortening (TS) into two terms: the minimum amount of shortening estimated from balanced cross-sections (MS) and missing shortening by erosion of the hanging-wall cut-offs (HMC). That is,

$$TS = MS + EHWC. \quad (1)$$

We could make meaningful comparison of the total amount of shortening between the central and eastern Himalaya,

Table 1. U–Pb geochronologic analyses

Sample	U (ppm)	$^{206}Pb/^{204}Pb$	U/Th	Isotopic ratio				Error correction	Apparent age (Ma)						Percent concentration
				$^{207}Pb^*/^{235}U$	± (%)	$^{206}Pb^*/^{238}U$	± (%)		$^{206}Pb^*/^{238}U$	± (Ma)	$^{207}Pb^*/^{235}U$	± (Ma)	$^{206}Pb^*/^{207}Pb^*$	± (Ma)	
AY9160314A															
AY9160314A-93	364	22359	0.5	1.51645	3.07	0.15404	1.99	0.65	924	17	937	19	969	24	95
AY9160314A-25	323	8597	6.3	1.52597	6.99	0.15468	6.46	0.92	927	56	941	42	973	27	95
AY9160314A-96	136	7491	1.3	1.64513	5.55	0.16067	3.67	0.66	961	33	988	34	1049	42	92
AY9160314A-94	459	9006	0.9	1.67716	5.44	0.16239	4.94	0.91	970	44	1000	34	1066	23	91
AY9160314A-97	310	23717	1.4	1.78568	4.40	0.16994	3.55	0.81	1012	33	1040	28	1101	26	92
AY9160314A-29	253	10650	0.9	1.72261	3.90	0.16369	2.05	0.53	977	19	1017	25	1104	33	89
AY9160314A-95	558	4311	1.4	1.40066	5.67	0.13310	4.07	0.72	806	31	889	33	1104	39	73
AY9160314A-42	244	17601	2.8	1.85665	5.06	0.17519	4.41	0.87	1041	42	1066	33	1118	25	93
AY9160314A-33	92	7383	1.9	1.87403	4.80	0.17607	2.12	0.44	1046	20	1072	31	1126	43	93
AY9160314A-7	217	10553	5.0	1.85133	2.77	0.17326	1.52	0.55	1030	15	1064	18	1134	23	91
AY9160314A-77	163	7511	2.7	1.96453	5.98	0.18373	4.30	0.72	1087	43	1103	40	1135	41	96
AY9160314A-3	472	11650	2.8	1.69827	3.72	0.15839	2.89	0.78	948	25	1008	24	1141	23	83
AY9160314A-23	158	11207	1.8	2.00470	5.16	0.18684	3.33	0.64	1104	34	1117	34	1142	39	97
AY9160314A-84	258	16571	7.1	1.88669	4.82	0.17509	3.09	0.64	1040	30	1076	32	1151	37	90
AY9160314A-18	70	3025	1.1	1.94167	7.92	0.17894	4.37	0.55	1061	43	1096	52	1165	65	91
AY9160314A-85	1043	18663	0.4	1.94842	7.45	0.17911	7.29	0.98	1062	71	1098	49	1170	15	91
AY9160314A-37	207	23422	5.5	2.10058	5.44	0.18718	4.45	0.82	1106	45	1149	37	1231	31	90
AY9160314A-81	347	13425	6.5	1.72869	3.85	0.15314	1.94	0.50	919	17	1019	25	1242	33	74
AY9160314A-38	116	9668	3.8	2.24416	4.94	0.19872	3.64	0.74	1168	39	1195	34	1243	33	94
AY9160314A-28	150	8077	2.3	2.49089	3.43	0.21998	2.30	0.67	1282	27	1269	25	1248	25	103
AY9160314A-30	589	9605	1.4	1.20827	14.16	0.10663	14.01	0.99	653	86	804	76	1250	20	52
AY9160314A-76	119	11357	1.1	2.23210	6.68	0.19682	5.44	0.81	1158	57	1191	46	1252	38	93
AY9160314A-49	247	16544	4.3	2.29797	5.16	0.20240	3.80	0.74	1188	41	1212	36	1254	34	95
AY9160314A-50	62	2996	3.3	1.18681	7.31	0.10321	3.73	0.51	633	22	795	40	1278	61	50
AY9160314A-64	155	11679	5.8	2.54878	4.02	0.22167	3.40	0.85	1291	40	1286	29	1278	21	101
AY9160314A-90	466	25450	1.8	2.23985	2.60	0.19488	2.36	0.91	1148	25	1194	18	1278	11	90
AY9160314A-63	300	7863	5.0	2.36808	6.65	0.20590	2.61	0.39	1207	29	1233	46	1279	60	94
AY9160314A-92	110	10200	1.0	2.73863	4.77	0.23795	4.16	0.87	1376	51	1339	35	1280	23	108
AY9160314A-89	298	15701	4.3	2.59223	7.18	0.22335	6.85	0.95	1300	80	1298	51	1297	21	100
AY9160314A-91	206	18293	1.6	2.74228	4.61	0.23429	4.01	0.87	1357	49	1340	34	1313	22	103
AY9160314A-70	397	19213	3.1	2.43948	3.13	0.20817	2.56	0.82	1219	28	1254	22	1315	17	93
AY9160314A-46	320	13123	2.5	2.29046	4.81	0.19504	2.00	0.42	1149	21	1209	33	1319	42	87
AY9160314A-15	340	25452	3.5	2.77361	2.00	0.22886	1.63	0.81	1329	20	1349	15	1380	11	96
AY9160314A-68	96	2324	3.6	0.97286	13.83	0.07975	7.17	0.52	495	34	690	67	1393	113	36
AY9160314A-47	211	22573	3.3	2.83727	3.29	0.23229	2.34	0.71	1347	28	1365	24	1395	22	97
AY9160314A-31	272	11303	3.1	2.80730	3.21	0.22818	2.77	0.86	1325	33	1358	24	1409	15	94
AY9160314A-80	843	8163	2.7	2.39138	4.35	0.19431	3.91	0.90	1145	41	1240	31	1410	18	81
AY9160314A-5	225	9044	10.3	2.48095	3.47	0.20128	1.84	0.53	1182	20	1267	25	1413	28	84
AY9160314A-26	115	6627	2.0	3.11156	3.81	0.25243	1.95	0.51	1451	25	1436	29	1413	31	103
AY9160314A-8	463	12102	2.6	2.71852	3.25	0.21996	2.71	0.83	1282	31	1334	24	1418	17	90
AY9160314A-2	81	9569	1.0	2.85210	6.70	0.23055	5.44	0.81	1337	65	1369	49	1420	37	94
AY9160314A-9	293	16768	1.9	2.64645	2.66	0.21373	2.22	0.84	1249	25	1314	19	1421	14	88
AY9160314A-75	332	20505	3.7	2.18470	6.98	0.17638	2.50	0.36	1047	24	1176	48	1422	62	74
AY9160314A-54	197	17013	5.4	2.92290	2.52	0.23431	1.24	0.49	1357	15	1388	19	1436	21	94
AY9160314A-41	118	4145	0.5	2.32343	5.04	0.18605	2.22	0.44	1100	22	1220	35	1438	43	76
AY9160314A-4	900	2735	2.2	1.65264	6.48	0.13196	4.03	0.62	799	30	991	40	1443	48	55
AY9160314A-12	100	8312	2.7	3.06753	3.63	0.24499	1.65	0.45	1413	21	1425	27	1443	31	98
AY9160314A-100	173	16374	1.5	2.99537	5.62	0.23876	4.98	0.89	1380	62	1406	42	1446	25	95
AY9160314A-86	124	7093	1.2	2.38783	5.64	0.18839	3.88	0.69	1113	40	1239	40	1466	39	76
AY9160314A-61	243	13361	2.5	3.01039	5.56	0.23675	5.13	0.92	1370	63	1410	42	1472	20	93
AY9160314A-27	245	15016	1.4	3.03097	2.04	0.23773	0.84	0.41	1375	10	1415	16	1477	18	93
AY9160314A-99	262	16356	1.5	2.92603	2.97	0.22917	2.29	0.77	1330	28	1389	22	1480	18	90
AY9160314A-1	613	7446	0.3	1.35800	7.72	0.10482	7.26	0.94	643	44	871	44	1507	25	43
AY9160314A-20	71	10990	1.3	3.48515	5.38	0.26581	2.65	0.49	1520	36	1524	42	1530	44	99
AY9160314A-98	174	9798	1.5	2.51966	4.87	0.19025	3.92	0.81	1123	40	1278	35	1549	27	72
AY9160314A-74	897	10554	4.9	2.65624	8.74	0.19854	8.33	0.95	1168	88	1316	63	1568	25	74
AY9160314A-43	170	12155	1.7	3.05531	4.13	0.22749	3.28	0.79	1321	39	1422	31	1575	24	84

(*Cont…*)

Table 1. (*Contd…*)

Sample	U (ppm)	$^{206}Pb/^{204}Pb$	U/Th	Isotopic ratio $^{207}Pb^*/^{235}U$	± (%)	$^{206}Pb^*/^{238}U$	± (%)	Error correction	Apparent age (Ma) $^{206}Pb^*/^{238}U$	± (Ma)	$^{207}Pb^*/^{235}U$	± (Ma)	$^{206}Pb^*/^{207}Pb^*$	± (Ma)	Percent concentration
AY9160314A-79	236	2724	1.8	4.11156	5.90	0.30330	3.67	0.62	1708	55	1657	47	1592	43	107
AY9160314A-16	180	7795	6.8	3.60518	3.19	0.26420	1.56	0.49	1511	21	1551	25	1605	26	94
AY9160314A-11	337	19684	0.8	4.00348	1.44	0.29119	1.09	0.76	1648	16	1635	12	1619	9	102
AY9160314A-6	212	6312	1.9	3.42406	4.89	0.24844	4.18	0.86	1430	53	1510	38	1623	24	88
AY9160314A-45	87	5682	3.0	3.16772	8.78	0.22915	5.18	0.59	1330	62	1449	66	1629	66	82
AY9160314A-62	126	6454	1.6	3.64045	6.10	0.26339	5.46	0.90	1507	73	1558	47	1629	25	93
AY9160314A-13	62	2097	0.6	2.79168	8.66	0.20140	3.24	0.37	1183	35	1353	63	1634	75	72
AY9160314A-59	104	6860	0.8	3.06504	7.60	0.22109	1.32	0.17	1288	15	1424	57	1634	70	79
AY9160314A-32	275	11741	1.3	3.86102	4.23	0.27835	4.04	0.96	1583	57	1606	34	1635	12	97
AY9160314A-72	38	2827	4.0	3.67426	9.07	0.26488	2.97	0.33	1515	40	1566	70	1635	80	93
AY9160314A-83	354	21861	1.6	3.70266	2.71	0.26655	1.28	0.47	1523	17	1572	21	1638	22	93
AY9160314A-52	46	3291	0.6	3.81447	9.03	0.27402	7.13	0.79	1561	98	1596	70	1642	51	95
AY9160314A-40	267	4301	2.8	2.98617	5.28	0.21442	4.07	0.77	1252	46	1404	39	1643	31	76
AY9160314A-60	406	44302	1.6	3.94810	3.02	0.28239	2.92	0.97	1603	41	1624	24	1650	7	97
AY9160314A-65	197	12586	1.6	3.82966	4.20	0.27286	4.01	0.96	1555	55	1599	33	1657	11	94
AY9160314A-66	143	9172	1.8	3.43777	3.85	0.24474	2.61	0.68	1411	33	1513	30	1659	26	85
AY9160314A-19	66	5882	2.2	3.39514	4.29	0.24119	1.68	0.39	1393	21	1503	33	1663	37	84
AY9160314A-56	91	10251	1.8	3.59176	5.77	0.25513	5.14	0.89	1465	67	1548	45	1663	24	88
AY9160314A-48	107	10708	2.6	4.11384	7.63	0.29138	6.92	0.91	1648	100	1657	61	1668	30	99
AY9160314A-78	121	16585	1.2	3.96445	4.73	0.28038	4.18	0.88	1593	59	1627	38	1671	20	95
AY9160314A-44	284	34950	2.1	4.16565	3.70	0.29307	3.26	0.88	1657	48	1667	30	1680	16	99
AY9160314A-17	77	14590	1.1	3.89828	3.76	0.27383	2.90	0.77	1560	40	1613	30	1683	22	93
AY9160314A-24	115	7411	2.2	3.91102	3.20	0.27458	2.27	0.71	1564	32	1616	26	1684	21	93
AY9160314A-14	63	7924	1.3	4.20492	6.56	0.29429	3.81	0.58	1663	56	1675	52	1690	49	98
AY9160314A-73	199	28659	1.3	4.40542	3.10	0.30668	2.87	0.92	1724	43	1713	25	1700	11	101
AY9160314A-71	81	11405	2.3	4.42981	4.34	0.30725	3.05	0.70	1727	46	1718	35	1707	28	101
AY9160314A-67	79	7406	1.9	3.63597	5.38	0.25197	3.63	0.68	1449	47	1557	42	1708	36	85
AY9160314A-88	97	10961	2.7	3.27270	7.21	0.22562	6.68	0.93	1312	79	1475	55	1718	25	76
AY9160314A-82	270	7502	3.8	3.52090	5.26	0.24232	4.58	0.87	1399	57	1532	41	1721	24	81
AY9160314A-39	183	16123	1.7	4.46301	3.62	0.30278	3.41	0.94	1705	51	1724	30	1747	11	98
AY9160314A-69	104	7887	2.4	3.27671	5.78	0.22207	3.93	0.68	1293	46	1476	44	1749	39	74
AY9160314A-55	119	16219	2.2	4.35275	5.35	0.28817	4.76	0.89	1632	68	1703	43	1792	22	91
AY9160314A-34	139	18445	1.4	4.33949	4.04	0.28620	3.01	0.74	1623	43	1701	33	1799	25	90
AY9160314A-22	253	6474	2.1	3.57547	3.77	0.23478	2.93	0.78	1360	36	1544	30	1807	22	75
AY9160314A-10	247	11623	6.0	4.49310	4.56	0.28292	3.73	0.82	1606	53	1730	37	1883	24	85
AY9160314A-36	112	12037	1.5	4.78239	4.98	0.29152	4.05	0.81	1649	59	1782	41	1941	26	85
AY9160314A-87	141	22914	2.8	5.64467	4.77	0.32792	3.07	0.64	1828	49	1923	40	2027	32	90
AY9160314A-58	168	8925	1.7	4.91287	4.97	0.27417	2.95	0.59	1562	41	1805	41	2097	35	74
AY9160314A-57	561	45522	2.3	7.61412	3.81	0.36651	2.41	0.63	2013	42	2187	34	2354	25	86
AY9160314A-35	276	44732	1.8	9.11317	2.55	0.42581	2.50	0.98	2287	48	2349	23	2404	4	95
AY9160314A-21	75	10917	0.8	9.68633	1.52	0.45188	0.87	0.57	2404	18	2405	14	2407	11	100
AY9160314A-51	81	5838	1.2	9.89737	4.32	0.42562	3.36	0.78	2286	64	2425	39	2544	23	90
AY9160314A-53	161	27736	19.8	14.46609	2.06	0.51055	1.71	0.83	2659	37	2781	19	2870	9	93
AY9170315														#DIV/0!	
AY9170315-4	811	2498	0.5	1.10520	8.52	0.11390	3.96	0.47	695	26	756	44	939	77	74
AY9170315-76	151	3200	2.3	1.41928	10.64	0.14476	6.55	0.62	872	53	897	62	961	86	91
AY9170315-1	199	6361	1.7	1.60096	4.66	0.16303	1.32	0.28	974	12	971	29	964	46	101
AY9170315-15	49	1380	1.3	1.45026	14.49	0.14654	1.96	0.14	882	16	910	84	980	146	90
AY9170315-59	346	22830	1.9	1.60846	4.16	0.16198	3.51	0.84	968	32	974	26	986	23	98
AY9170315-13	1055	1667	2.9	0.77928	10.90	0.07818	2.86	0.26	485	13	585	47	994	107	49
AY9170315-6	646	2309	1.7	1.17344	10.37	0.11745	6.22	0.60	716	42	788	55	999	84	72
AY9170315-53	205	17120	5.0	1.69084	4.28	0.16806	2.51	0.59	1001	23	1005	27	1013	35	99
AY9170315-84	120	4192	2.0	1.72207	7.79	0.17037	5.10	0.65	1014	48	1017	49	1023	60	99
AY9170315-94	296	14193	6.3	1.70231	2.69	0.16831	1.47	0.55	1003	14	1009	17	1024	23	98
AY9170315-23	169	8427	3.4	1.62236	4.20	0.16029	2.27	0.54	958	20	979	26	1025	36	94
AY9170315-10	143	6546	3.1	1.65739	5.95	0.16343	1.85	0.31	976	17	992	37	1029	57	95
AY9170315-64	268	9071	3.2	1.75550	4.22	0.16998	3.52	0.83	1012	33	1029	27	1066	23	95
AY9170315-20	1416	3442	2.5	1.33886	6.00	0.12907	3.04	0.51	783	22	863	34	1075	52	73

(*Cont…*)

Table 1. (*Contd…*)

Sample	U (ppm)	$^{206}Pb/^{204}Pb$	U/Th	Isotopic ratio $^{207}Pb^*/^{235}U$	± (%)	$^{206}Pb^*/^{238}U$	± (%)	Error correction	Apparent age (Ma) $^{206}Pb^*/^{238}U$	± (Ma)	$^{207}Pb^*/^{235}U$	± (Ma)	$^{206}Pb^*/^{207}Pb^*$	± (Ma)	Percent concentration
AY9170315-3	743	11644	10.0	1.54557	2.64	0.14732	1.94	0.74	886	16	949	16	1097	18	81
AY9170315-44	47	3228	1.2	1.92730	11.44	0.18325	4.31	0.38	1085	43	1091	74	1102	106	98
AY9170315-40	294	13627	2.9	1.74461	3.06	0.16567	2.28	0.74	988	21	1025	20	1105	20	89
AY9170315-91	2469	470	43.9	1.53100	26.31	0.14526	4.20	0.16	874	34	943	150	1107	259	79
AY9170315-41	320	25128	2.5	2.02739	2.69	0.19156	2.22	0.83	1130	23	1125	18	1115	15	101
AY9170315-37	478	2932	0.9	1.65603	8.58	0.15636	3.53	0.41	937	31	992	53	1116	78	84
AY9170315-77	270	1994	0.9	1.47678	10.28	0.13903	6.17	0.60	839	48	921	60	1122	82	75
AY9170315-74	260	2114	0.3	1.36284	11.13	0.12785	6.48	0.58	776	47	873	63	1129	90	69
AY9170315-93	425	16432	3.1	2.10237	2.69	0.19709	1.85	0.69	1160	20	1150	18	1131	19	103
AY9170315-65	698	6455	1.3	1.80536	8.06	0.16750	7.59	0.94	998	70	1047	51	1151	27	87
AY9170315-5	71	2194	1.0	1.69529	13.07	0.15517	6.81	0.52	930	59	1007	80	1178	110	79
AY9170315-7	219	12068	2.0	2.01720	4.21	0.18423	3.78	0.90	1090	38	1121	28	1182	18	92
AY9170315-50	234	11623	1.7	2.22353	4.08	0.20104	3.45	0.85	1181	37	1189	28	1202	21	98
AY9170315-12	879	5058	0.6	1.55629	7.35	0.14062	6.24	0.85	848	49	953	45	1204	38	70
AY9170315-83	83	4089	1.3	2.21685	5.18	0.20024	1.59	0.31	1177	17	1186	36	1204	49	98
AY9170315-92	251	7120	3.9	2.12402	3.78	0.19048	2.10	0.56	1124	22	1157	26	1218	31	92
AY9170315-88	481	17697	0.8	2.33424	8.80	0.20830	8.55	0.97	1220	94	1223	61	1228	21	99
AY9170315-19	1148	10754	5.0	2.15514	3.76	0.19106	3.38	0.90	1127	35	1167	26	1241	16	91
AY9170315-62	157	13825	2.2	2.31696	9.22	0.20431	8.29	0.90	1198	90	1218	63	1251	39	96
AY9170315-45	200	12085	2.7	2.45845	5.84	0.21655	5.38	0.92	1264	61	1260	41	1254	22	101
AY9170315-96	106	7644	3.3	2.47905	3.94	0.21781	2.52	0.64	1270	29	1266	28	1259	30	101
AY9170315-36	118	3770	4.6	2.52264	12.16	0.22119	5.74	0.47	1288	67	1279	85	1263	105	102
AY9170315-47	54	5127	1.2	2.51692	7.63	0.21926	4.54	0.59	1278	52	1277	54	1275	60	100
AY9170315-69	287	3359	0.8	1.91140	8.67	0.16623	7.04	0.81	991	64	1085	56	1278	49	78
AY9170315-75	92	4160	1.8	2.36703	6.28	0.20500	3.84	0.61	1202	42	1233	44	1287	48	93
AY9170315-8	103	6256	3.7	2.29180	5.44	0.19774	3.05	0.56	1163	32	1210	38	1294	44	90
AY9170315-97	504	4732	0.9	2.06562	4.00	0.17728	2.02	0.51	1052	20	1138	27	1304	33	81
AY9170315-100	206	10327	1.5	2.58752	5.35	0.21965	4.84	0.90	1280	56	1297	39	1326	22	97
AY9170315-39	374	22363	1.7	2.77947	2.98	0.23538	2.68	0.90	1363	33	1350	22	1330	13	102
AY9170315-43	98	8634	1.6	2.77028	5.78	0.23240	2.04	0.35	1347	25	1348	42	1348	52	100
AY9170315-60	173	10799	2.1	2.48054	6.38	0.20665	4.93	0.77	1211	54	1266	45	1362	39	89
AY9170315-34	479	2081	1.6	1.51721	7.36	0.12585	2.47	0.33	764	18	937	44	1370	67	56
AY9170315-26	208	3570	1.4	2.39715	7.41	0.19862	4.16	0.56	1168	44	1242	52	1372	59	85
AY9170315-31	107	6885	2.3	2.81256	4.97	0.23300	3.76	0.76	1350	46	1359	37	1373	31	98
AY9170315-49	423	9886	3.2	2.64785	4.94	0.21933	4.63	0.94	1278	54	1314	36	1373	17	93
AY9170315-98	602	35760	5.3	2.94616	2.25	0.24337	2.00	0.89	1404	25	1394	17	1378	10	102
AY9170315-16	101	5781	16.0	2.86788	4.20	0.23671	1.90	0.45	1370	23	1374	31	1380	36	99
AY9170315-51	44	3217	1.8	2.58348	15.99	0.21293	13.12	0.82	1244	147	1296	111	1382	88	90
AY9170315-46	126	5771	1.9	2.87867	6.98	0.23612	6.18	0.89	1367	76	1376	51	1392	31	98
AY9170315-32	114	5556	1.5	2.72375	4.60	0.22307	2.79	0.61	1298	33	1335	34	1395	35	93
AY9170315-14	29	1037	2.1	1.94255	16.06	0.15706	4.29	0.27	940	37	1096	102	1419	148	66
AY9170315-48	172	4682	1.4	2.76699	7.08	0.22237	5.83	0.82	1294	68	1347	52	1431	38	90
AY9170315-80	256	10423	2.0	3.22119	4.44	0.25247	3.96	0.89	1451	51	1462	34	1478	19	98
AY9170315-52	827	10044	4.5	2.54291	3.48	0.19910	3.14	0.90	1171	34	1284	25	1480	14	79
AY9170315-67	93	7322	1.8	3.20032	6.45	0.23693	5.44	0.84	1371	67	1457	49	1586	32	86
AY9170315-87	716	31081	0.9	3.77886	2.18	0.27873	2.09	0.96	1585	29	1588	17	1593	6	99
AY9170315-71	335	7062	1.5	3.44604	6.57	0.25313	6.19	0.94	1455	80	1515	51	1600	21	91
AY9170315-30	160	9385	1.2	3.74412	4.86	0.27447	4.32	0.89	1564	60	1581	38	1604	21	97
AY9170315-18	592	16850	6.0	3.63091	2.72	0.26575	2.51	0.92	1519	34	1556	22	1607	10	95
AY9170315-27	362	19172	0.9	3.59975	2.04	0.26307	1.75	0.86	1506	24	1550	16	1610	10	94
AY9170315-38	195	12469	2.2	2.95673	6.50	0.21580	5.72	0.88	1260	65	1397	48	1612	29	78
AY9170315-63	539	12180	2.1	3.61102	3.34	0.26281	2.97	0.89	1504	40	1552	26	1618	14	93
AY9170315-82	172	12157	1.4	3.75141	2.73	0.27058	1.72	0.63	1544	24	1582	22	1634	20	94
AY9170315-54	123	5818	0.9	3.80905	5.70	0.27452	4.75	0.83	1564	66	1595	45	1636	29	96
AY9170315-66	74	8764	1.7	3.96676	7.33	0.28503	6.53	0.89	1617	93	1627	58	1641	31	99
AY9170315-89	161	7201	1.8	2.51226	8.00	0.17999	7.56	0.95	1067	74	1276	57	1647	24	65
AY9170315-11	108	7274	1.3	3.86294	2.31	0.27651	1.02	0.44	1574	14	1606	18	1648	19	95
AY9170315-33	156	9649	3.2	3.71812	5.85	0.26482	5.31	0.91	1515	71	1575	46	1658	23	91

(*Cont…*)

Table 1. (*Contd…*)

Sample	U (ppm)	$^{206}Pb/^{204}Pb$	U/Th	Isotopic ratio $^{207}Pb^*/^{235}U$	± (%)	$^{206}Pb^*/^{238}U$	± (%)	Error correction	Apparent age (Ma) $^{206}Pb^*/^{238}U$	± (Ma)	$^{207}Pb^*/^{235}U$	± (Ma)	$^{206}Pb^*/^{207}Pb^*$	± (Ma)	Percent concentration
AY9170315-86	442	14383	0.8	3.96533	1.84	0.28147	1.41	0.77	1599	20	1627	15	1664	11	96
AY9170315-42	146	10203	2.2	3.73860	6.64	0.26424	6.09	0.92	1512	82	1580	52	1672	24	90
AY9170315-72	64	7198	1.1	3.85398	7.02	0.27113	6.00	0.85	1547	82	1604	55	1681	34	92
AY9170315-9	61	2969	2.0	3.77136	5.10	0.26473	1.52	0.30	1514	21	1587	40	1685	45	90
AY9170315-90	93	5324	1.7	3.48196	5.11	0.24256	4.07	0.80	1400	51	1523	40	1699	28	82
AY9170315-29	122	5092	1.3	4.10027	7.59	0.28527	6.28	0.83	1618	89	1654	60	1701	39	95
AY9170315-85	280	21336	0.5	4.28567	5.11	0.29825	4.98	0.98	1683	73	1691	41	1701	10	99
AY9170315-17	39	811	1.6	3.36320	15.48	0.23384	5.72	0.37	1355	70	1496	114	1702	132	80
AY9170315-57	96	16245	2.1	4.31576	2.49	0.29803	1.74	0.70	1682	26	1696	20	1715	16	98
AY9170315-81	124	11288	1.7	4.30078	3.69	0.29565	2.68	0.73	1670	39	1694	30	1723	23	97
AY9170315-25	104	7744	1.7	4.36159	3.92	0.29897	2.75	0.70	1686	41	1705	32	1728	26	98
AY9170315-68	49	4246	2.1	4.37748	5.17	0.29914	2.43	0.47	1687	36	1708	42	1734	42	97
AY9170315-70	254	8054	1.2	3.47238	3.53	0.23604	2.86	0.81	1366	35	1521	27	1744	19	78
AY9170315-24	89	4659	1.9	4.56429	4.96	0.30298	3.74	0.75	1706	56	1743	41	1787	30	95
AY9170315-28	43	2010	1.6	2.81715	13.05	0.18309	5.01	0.38	1084	50	1360	93	1826	109	59
AY9170315-61	102	13486	2.2	4.76500	8.91	0.30466	8.33	0.94	1714	124	1779	72	1855	28	92
AY9170315-2	271	18445	8.7	4.80024	2.79	0.30286	2.30	0.83	1706	34	1785	23	1879	14	91
AY9170315-95	1131	25365	11.0	4.59710	3.12	0.28848	3.03	0.97	1634	44	1749	26	1889	7	86
AY9170315-22	63	8373	1.2	5.36226	4.07	0.32944	2.43	0.60	1836	39	1879	34	1927	29	95
AY9170315-21	57	6752	0.7	5.52704	7.73	0.33505	6.22	0.81	1863	100	1905	64	1951	41	95
AY9170315-58	55	6324	1.4	5.53059	3.58	0.32696	2.82	0.79	1824	45	1905	30	1996	20	91
AY9170315-35	265	16749	3.0	6.96732	3.58	0.33647	3.29	0.92	1870	53	2107	31	2348	12	80
AY9170315-55	191	22268	1.6	8.80751	8.62	0.41443	8.59	1.00	2235	160	2318	76	2392	6	93
AY9170315-99	119	8804	2.7	9.40897	4.52	0.43222	3.06	0.68	2316	59	2379	41	2433	28	95
AY9170315-56	149	22710	0.6	10.39014	2.67	0.46740	2.62	0.98	2472	54	2470	25	2469	4	100

$^{206}Pb/^{204}Pb$ is measured ratio.
All uncertainties are at the 1s level and include only random (measurement) errors.
U concentration and U/Th have uncertainties of ~25%.
Decay constants: $^{235}U = 9.8485 \times 10^{-10}$. $^{238}U = 1.55125 \times 10^{-10}$, $^{238}U/^{235}U = 137.88$.
Isotope ratios are corrected for Pb/U fractionation by comparison with standard zircon with an age of 564 ± 4 Ma (2s).
Initial Pb composition interpreted from Stacey and Kramers (1975), with uncertainties of 1.0 for $^{206}Pb/^{204}Pb$ and 0.3 for $^{207}Pb/^{204}Pb$.

Table2. Ion microprobe data analysis *in situ* monazite dates from AY091403-(8a) sample

Age (Ma) ^{204}Pb corrected	$^{208}Pb/^{232}Th$ 1s.e.	sample no.
10.32	2.83	8a-1@1.ais
10.03	0.813	8a-3@2.ais
10.13	2.35	8a-4.ais
9.825	2.7	8a-5@4.ais
13.38	7	g2-m11.ais

Weighted mean age $1/s^2$	Age*$1/s^2$	MSWD (Age – weighted mean age)$^2/s^2$
0.124861092	1.28856647	0.007321711
1.512930258	15.17469049	0.003463373
0.181077411	1.834314169	0.000492549
0.137174211	1.347736626	0.008769656
0.020408163	0.273061224	0.222535204
sum	sum	sum
1.976451136	19.91836898	0.242582494

Weighted mean age (Ma)	1 s.e.	MSWD
10.0778454	0.002520533	0.060645623

if we know the relative magnitude of EHWC in the two regions. As erosion is directly related to precipitation, which currently decreases westward along the Himalaya[56], we may infer the magnitude of erosion in the eastern Himalaya to be greater than that in the central and western Himalaya, if the current precipitation pattern persisted in the Neogene. This assumption leads to the following inequality:

EHMC (eastern Himalaya) > EHMC (central Himalaya). (2)

Because

TS (eastern Himalaya) = MS (eastern Himalaya) + EHMC (eastern Himalaya), (3)

TS (central Himalaya) = MS (central Himalaya) + EHMC (central Himalaya), (4)

and

MS (eastern Himalaya) > MS (central Himalaya), (5)

we have

$$\text{TS (eastern Himalaya)} > \text{TS (central Himalaya)}. \quad (6)$$

That is, the total amount of shortening in the eastern Himalaya is greater than that in the central Himalaya. Another implicit assumption in the above inference is that the shortening in the central and eastern Tethyan Himalaya is constant along strike, which is supported by early studies[49,50].

Despite the high uncertainties in our estimates of the total amount of crustal shortening across the Arunachal Himalaya, there is little doubt that the Himalayan orogen did not develop in a symmetric manner, in which crustal shortening decreases laterally from the central to the east and west. The easternmost part of the Himalayan orogen must have significantly more crustal shortening than the western Himalaya. Our interpreted westward decrease in crustal shortening supports the early inference by Guillot *et al*.[57], who relate the variation of shortening to the westward decrease in convergence rate between India and Asia[13,14]. Future research may expand our study by examining how strain is distributed in the whole Himalayan–Tibetan orogen in response to the relative Cenozoic rotation between India and Asia. Recognition of an MCT tectonic window inside the eastern Himalaya suggests that (1) the MCT is broadly folded, a case widely recognized elsewhere in the Himalaya and has been particularly noted in western Bhutan[16] but has been uncertain in the Arunachal Himalaya (c.f. refs 26 and 30), and (2) the GHC is quite thin (i.e. <7–10 km) when projecting the STD[4] from easternmost Bhutan onto our cross-section in western Arunachal.

Detrital zircon analysis indicates that the Lesser Himalayan metasedimentary sequence (the Rupa Group) must be younger than 950 Ma. The age relationship between the Rupa Group and the Bomdila orthogneiss is currently unclear. However, radiometric dating of the augen gneiss in the near future will resolve this problem. That is, we will know whether the Bomdila gneiss was the basement of the Rupa Group or it has intruded into the metasedimentary sequence.

Conclusion

Geologic mapping across the westernmost Arunachal Himalaya reveals the presence of an MCT window and a prominent north-trending, active rift that cuts and offsets the MCT.

Detrital zircon analysis indicates that the Lesser Himalayan metasedimentary sequence (the Rupa Group) must be younger than 950 Ma.

The MCT in the Arunachal Himalaya was active at about 10 Ma, but its initiation and termination ages remain unknown.

The GHC in the Arunachal Himalaya has been thickened by ductile thrusting as represented by the Zimithang ductile thrust zone mapped by this study.

The total amount of shortening across the Arunachal Himalaya is at least 500 km. This magnitude of shortening is definitely greater than that estimated in the northern Pakistan Himalaya around 200 km and probably also exceeds the amount of shortening across the central Himalaya in Nepal. The apparent westward decrease in the magnitude of crustal shortening along the Himalayan orogen may result from relative rotation of India with Asia during the Indo-Asian collision and suggests that the development of the Himalayan orogen on a timescale of tens of million years is asymmetric.

1. Gansser, A., *The Geology of the Himalayas*, Wiley Interscience, New York, 1964.
2. Searle, M. P. Waters, D. J., Dransfield, M. W., Stephenson, B. J., Walker, C. B., Walker, J. D. and Rex, D. C., Thermal and mechanical models for the structural and metamorphic evolution of the Zanskar High Himalaya. In *Continental Tectonics* (eds MacNiocaill, C. and Ryan, P. D.), Geological Society of London Special Publication, 1999, vol. 164, pp. 139–156,.
3. DeCelles, P. G., Robinson, D. M., Quade, J., Ojha, T. P., Garzione, C. N., Copeland, P. and Upreti, B. N., Stratigraphy, structure, and tectonic evolution of the Himalayan fold-thrust belt in western Nepal. *Tectonics*, 2001, **20**, 487–509.
4. Grujic, D., Hollister, L. S. and Parrish, R.R., Himalayan metamorphic sequence as an orogenic channel: insight from Bhutan. *Earth Planet. Sci. Lett*., 2002, **198**, 177–191.
5. Steck, A., Geology of the NW Indian Himalaya. *Eclogae Geol. Helv*., 2003, **96**, 147–213.
6. DiPietro, J., Pogue, K. R., Hussain, A. and Ahmad, I., Geological map of the Indus syntaxis and surrounding area, northwest Himalaya, Pakistan. In *Himalaya and Tibet: Mountain Roots to Mountain Tops* (eds Macfarlane, A., Sorkhabi, R. B. and Quade, J.), Geological Society of America Special Papers, Boulder, Colorado, 1999, vol. 328, pp. 159–178.
7. Pogue, K. R., Hylland, M. D., Yeats, R. S., Khattak, W. U. and Hussain, A., Stratigraphic and structural framework of Himalayan foothills, northern Pakistan. In *Himalaya and Tibet: Mountain Roots to Mountain Tops* (eds Macfarlane, A., Sorkhabi, R. B. and Quade, J.), Geological Society of America Special Papers, Boulder, Colorado, 1999, vol. 328, pp. 257–274.
8. Le Fort, P., Evolution of the Himalaya. In *The Tectonic Evolution of Asia* (eds Yin, A. and Harrison, T. M.), Cambridge University Press, New York, 1996, pp. 95–106.
9. Thakur, V. C., Structure of the Chamba nappe and position of the Main Central Thrust in Kashmir Himalaya. *J. Asian Earth Sci*., 1998, **16**, 269–282.
10. DiPietro, J. A. and Pogue, K. R., Tectonostratigraphic subdivisions of the Himalaya: A view from the west. *Tectonics*, 2004, **23**, doi: 10.1029/2003TC001554.
11. Yin, A., Tectonic evolution of the Himalayan orogen as constrained by along-strike variation of structural geometry, exhumation history, and foreland sedimentation. *Earth-Sci. Rev.*, in press.
12. Steck, A., Geology of the NW Indian Himalaya. *Eclogae Geol. Helv.*, 2003, **96**, 147–213.
13. Patriat, P. and Achache, J., India–Eurasia collision chronology has implications for crustal shortening and driving mechanism of plates. *Nature*, 1984, **311**, 615–621.
14. Dewey, J. F., Cande, S. and Pitman, W. C., Tectonic evolution of the India–Eurasia collision zone. *Eclogae Geol. Helv*., 1989, **82**, 717–734.
15. Gansser, A., *Geology of the Bhutan Himalaya*, Birkhäuser Verlag, Boston, 1983.
16. Bhargava, O. N., *The Bhutan Himalaya: A Geological Account*, Geological Survey of India Special Publication, 1995, vol. 39.
17. Godwin-Austin, H. H., Notes on the geology of the Dafla Hills, Assam, lately visited by the Force under Brigadier-General Stafford, C.S. *J. Asiat. Soc. Bengal*, 1875**,** **44**, 34–41.

18. La Touche, T. D., Notes on the geology of the Aka Hills, Assam. *Rec. Geol. Surv. India*, 1885, **18**, 121–124.
19. MaClaren, J. M., Geology of Upper Assam. *Rec. Geol. Surv. India*, 1904, **31**, 179–204.
20. Brown, C. J., A geologic reconnaissance through the Dihang Valley, being the geological result of the Abor Expedition, 1911–12. *Rec. Geol. Surv. India*, 1912, **42**, 231–264.
21. Jain, A. K., Thakur, V. C. and Tandon, S. K., Stratigraphy and structure of the Siang district, Arunachal (NEFA) Himalaya. *Himalayan Geol*., 1974, **4**, 28–60.
22. Verma, P. K. and Tandon, S. K., Geological observations in parts of Kameng district, Arunachal Pradesh (NEFA). *Himalayan Geol*., 1976, **6**, 259–286.
23. Acharyya, S. K., Ghosh, S. C., Ghosh, R. N. and Shah, S. C., The Gondwana Group and associated marine sequences of Arunachal Pradesh (NEFA), Eastern Himalaya. *Himalayan Geol*., 1975, **5**, 60–80.
24. Jangpangi, B. S., Stratigraphy and tectonics of parts of eastern Bhutan. *Himalayan Geol*., 1974, **4**, 117–136.
25. Thakur, V. C., Tectonic zonation and regional framework of eastern Himalaya. *Sci. Terre, Mem.*, 1986, 47, 347–360.
26. Singh, S. and Chowdhary, P. K., An outline of the geological framework of the Arunachal Himalaya. *J. Himalayan Geol*., 1990, **1**, 189–197.
27. Acharyya, S. K., The Cenozoic foreland basin and tectonics of the eastern sub-Himalaya: Problems and prospects. *Himalayan Geol*., 1994, **15**, 3–21.
28. Acharyya, S. K., Structural framework and tectonic evolution of the eastern Himalaya. *Himalayan Geol*., 1980, **10**, 412–439.
29. Acharyya, S. K., Thrust tectonics and evolution of domes and the syntaxis in eastern Himalaya, India. *J. Nepal. Geol. Soc*., 1998, **18**, 1–17.
30. Kumar, G., *Geology of Arunachal Pradesh*, Geological Society of India, Bangalore, 1997.
31. Thakur, V. C. and Jain, A. K., Tectonics of the region of eastern Himalayan syntaxis. *Curr. Sci.*, 1974, **43**, 783–785.
32. Geological Survey of India, Geological and mineral map of NE India at a scale of 1 : 2 M. 1998.
33. Srinivasan, V., Litho-stratigraphy and structure of the low-grade metasedimentaries in western part of the Arunachal Pradesh. *Himalayan Geol*., 1999, **20**, 53–60.
34. Tripathi, C., Dungrakoti, B. D., Jains, L. S., Kaura, S. C., Basu, S. and Laxmipathi, N. S., Geology of Dirange–Doimara area, Kameng District, Arunachal Pradesh with special reference to structure and tectonics. *Himalayan Geol*., 1982, **10**, 353–365.
35. Krishnan, M. S., General report of the geological survey of India for year 1953. *Rec. Geol. Surv. India*, 1958, **87**, 46–47.
36. Bhalla, J. K. and Bishui, P. K., Geochronology and geochemistry of granite emplacement and metamorphism in northeastern Himalaya. *Rec. Geol. Surv. India*, 1989, **122**, 18–20.
37. Dikshitulu, G. R., Pandey, B. K., Krishna, V. and Dhana, R., Rb–Sr systematics of granitoids of the Central Gneissic Complex, Arunachal Himalaya: Implications on tectonics, stratigraphy, and source. *J. Geol. Soc. India*, **45**, 51–56.
38. Parrish, R. R. and Hodges, K. V., Isotopic constraints on the age and provenance of the Lesser and Greater Himalayan sequences, Nepalese Himalaya. *Geol. Soc. Am. Bull.*, 1996, **108**, 904–911.
39. DeCelles, P. G., Gehrels, G. E., Quade, J., LaReau, B. and Spurlin, M., Tectonic implications of U–Pb zircon ages of the Himalayan orogenic belt in Nepal. *Science*, 2000, **288**, 497–499.
40. Lovera, O. M., Grove, M., Kimbrough, D. L. and Abbott, P. L., A method for evaluating basement exhumation histories from closure age distributions of detrital minerals. *J. Geophys. Res.*, 1999, **104**, 29,419–29,438.
41. Harrison, T. M., Grove, M., McKeegan, K. D., Coath, C. D., Lovera, O. M. and Le Fort, P., Origin and episodic emplacement of the Manaslu intrusive complex, central Himalaya. *J. Petrol*., 1999, **40**, 3–19.
42. Harrison, T. M., McKeegan, K. D. and LeFort, P., Detection of inherited monazite in the Manaslu leucogranite by Pb-208/Th-232 ion microprobe dating – Crystallization age and tectonic implications. *Earth Planet. Sci. Lett*., 1995, **133**, 271–282.
43. Harrison, T. M., Ryerson, F. J., LeFort, P., Yin, A., Lovera, O. M. and Catlos, E. J., A Late Miocene–Pliocene origin for the Central Himalayan inverted metamorphism. *Earth Planet. Sci. Lett*., 1997, **146**, E1–E8.
44. Catlos, E. J., Harrison, T. M., Kohn, M. J., Grove, M., Ryerson, F. J., Manning, C. E. and Upreti, B. N., Geochronologic and thermobarometric constraints on the evolution of the Main Central Thrust, central Nepal Himalaya. *J. Geophys. Res*., 2001, **106**, 16177–16204.
45. Coward, M. P. and Butler, R. H. W., Thrust tectonics and the deep structure of the Pakistan Himalaya. *Geology*, 1985, **13**, 417–420.
46. Corfield, R. L. and Seale, M. P., Crustal shortening across the north Indian continental margin, Ladakh, India. In *Tectonics of the Nanga Parbat Syntaxis and the Western Himalaya* (eds Khan, M. A. *et al*.), The Geological Society Special Publication, 2000, vol. 170, pp. 395–410.
47. Wiesmayr, G. and Grasemann, B., Eohimalayan fold and thrust belt: Implications for the geodynamic evolution of the NW-Himalaya (India). *Tectonics*, 2002, **2**, 1058.
48. Srivastava, P. and Mitra, G., Thrust geometries and deep structure of the outer and lesser Himalaya, Kumoan and Garhwal (India): Implications for evolution of the Himalayan fold and thrust belt. *Tectonics*, 1994, **13**, 89–109.
49. Ratschbacher, L., Frisch, W., Liu, G. and Chen, C., Distributed deformation in southern and western Tibet during and after the India–Asia collision. *J. Geophys. Res.*, 1994, **99**, 19,817–19,945.
50. Murphy, M. A. and Yin, A., Structural evolution and sequence of thrusting in the Tethyan fold-thrust belt and Indus–Yalu suture zone, southwest Tibet. *Geol. Soc. Am. Bull*., 2003, **115**, 21–34.
51. Schelling, D. and Arita, K., Thrust tectonics, crustal shortening, and the structure of the far-eastern Nepal, Himalaya. *Tectonics*, 1991, **10**, 851–862.
52. Lavé, J. and Avouac, J. P., Active folding of fluvial terraces across the Siwaliks Hills, Himalayas of central Nepal. *J. Geophys. Res.*, 2000, **105**, 5735–5770.
53. Sharma, B. and Ratnam, C., Use of gravity data to resolve complex fold structure in the sub-Himalayan region of upper Assam. *Himalayan Geol*., 1974, **4**, 61–73.
54. Dahlstrom, C. D. A., Balanced cross-sections. *Can. J. Earth Sci*., 1969, **6**, 743–757.
55. Laubscher, J. P., Ein Fernschubhypothese der Jurafaltung. *Ecologae Geol. Helv*., 1961, **54**, 221–282.
56. Finlayson, D. P., Montgomery, D. R. and Hallet, B., Spatial coincidence of rapid inferred erosion with young metamorphic massifs in the Himalayas. *Geology*, 2002, **30**, 219–222.
57. Guillot, S., Cosca, M., Allemand, P. and LeFort, P., Contrasting metamorphic and geochronologic evolution along the Himalayan belt. In *Himalaya and Tibet: Mountain Roots to Mountain Tops* (eds Macfarlane, A., Sorkhabi, R. B. and Quade, J.), Geological Society of America Special Papers, Boulder, Colorado, 1999, vol. 328, pp. 117–128.
58. Ding, L., Zhong, D. L., Yin, A., Kapp, P. and Harrison, T. M., Cenozoic structural and metamorphic evolution of the eastern Himalayan syntaxis (Namche Barwa). *Earth Planet. Sci. Lett*., 2001, **192**, 423–438.
59. Tripathi, C. and Kaura, S. C., A note on the metamorphites of Arunachal Pradesh. *Geol. Surv. India Spec. Publ*., 1998, **22**, 45–52.
60. Yin, A. and Harrison, T. M., Geologic evolution of the Himalayan–Tibetan orogen. *Annu. Rev. Earth Planet. Sci*., 2000, **28**, 211–280.
61. Gehrels, G. E., DeCelles, P. G., Martin, A., Ojha, T. P., Pinhassi, G. and Upreti, B. N., Initiation of the Himalayan orogen as an early Paleozoic thin-skinned thrust belt. *GSA Today*, 2003, **13**, 4–9.

ACKNOWLEDGEMENTS. This work was supported by a grant from UCLA to A.Y., a faculty development grant to T.K.K. and a travel grant from SAP (UGC) to C.S.D. The ion-microprobe facilities at UCLA are partially supported by a grant from the Instrumentation and Facilities Program, Division of Earth Sciences, US National Science Foundation.

Received 20 December 2004; revised accepted 5 October 2005